Solid Freeform Fabrication 2018: Proceedings of the 29th Annual International Solid Freeform Fabrication Symposium – An Additive Manufacturing Conference
Reviewed Paper

The effect of processing parameter on zirconium modified Al-Cu-Mg alloys fabricated by selective laser melting

Xiaojia Nie[*], Hu Zhang[*,†], Haihong Zhu[*], Zhiheng Hu[*], Xiaoyan Zeng[*]

*Wuhan National Laboratory for Optoelectronics, Huazhong University of Science and Technology, Wuhan, Hubei, P.R. of China

†School of Optical and Electronic Information, Huazhong University of Science and Technology, Wuhan, Hubei, P.R. of China

Abstract

The newly designed alloy compositions for selective laser melting (SLM) have aroused great interest. In this study, zirconium modified Al-Cu-Mg alloys were fabricated by SLM. Results show that crack-free samples with relative density of nearly 100% were obtained by optimizing the processing parameters. With the increase of scanning speed, the relative density decreases due to insufficient energy input. In addition, the microstructure transforms from homogeneous to bio-modal, the reason is the unstable flows caused by the high scanning speed. The small hatching space will provide more energy input and preheat, leading to the coarse surface.

Introduction

Additive Manufacturing (AM) processes enable to fabricate parts with very complex shape[1]. Selective laser melting (SLM), one of the preferred AM techniques, has recently gained considerable attention due to high manufacturing flexibility, near-net-shape production and efficient use of raw material[2, 3]. Al-Cu-Mg alloy has become an attractive material due to the low density, high fracture toughness and fatigue strength[4, 5]. Nowadays, processing high strength aluminum alloys by SLM is confronted with great difficulties because of its poor flowability, high reflectivity, high thermal conductivity, large solidification range and hot cracking susceptibility[6]. Therefore, the biggest stumbling block to the application of high strength aluminum in SLM is the hot crack. To expand the scope of aluminum alloys suiting for SLM, new high strength aluminum alloys are urgent to be investigated.

Recently, scandium (Sc), zirconium (Zr), titanium (Ti) and vanadium (V) have been proved as the effective microalloying element for aluminum alloys to improve the weldability and mechanical properties[7-9]. Nowadays, the addition of microalloying element has been applied to SLM aluminum alloys to improve their formability. The microstructural evolution, densification, properties and heat treatment of Al-Mg-Sc-Zr fabricated by SLM have been investigated[10-13]. Zhang H et al.[14] have found that the Zr modified Al-Cu-Mg parts with ultrafine grain exhibits better mechanical properties and broader processing window. However, the effect of processing parameters on the Zr modified Al-Cu-Mg alloy has not been studied.

The present work investigated the effect of scanning speed and hatching space on Zr modified Al-Cu-Mg alloy fabricated by SLM. The relative density, surface roughness, microstructure and element distribution were discussed under different processing parameters.

Materials and experiment procedures

Materials

The spherical gas atomized Al-Cu-Mg powders with an average particle size of 36 μm was used in the experiments. The powder had a composition of 93.23 Al, 4.24 Cu, 1.97 Mg, and 0.56 Mn in wt.%. The Al-Cu-Mg powder mixture with zirconium particles were blended by mechanical mixing in an argon atmosphere for 4 h. The morphology of pure Zr powders and the Al-Cu-Mg powders mixture with 2% zirconium are shown in Fig. 1.

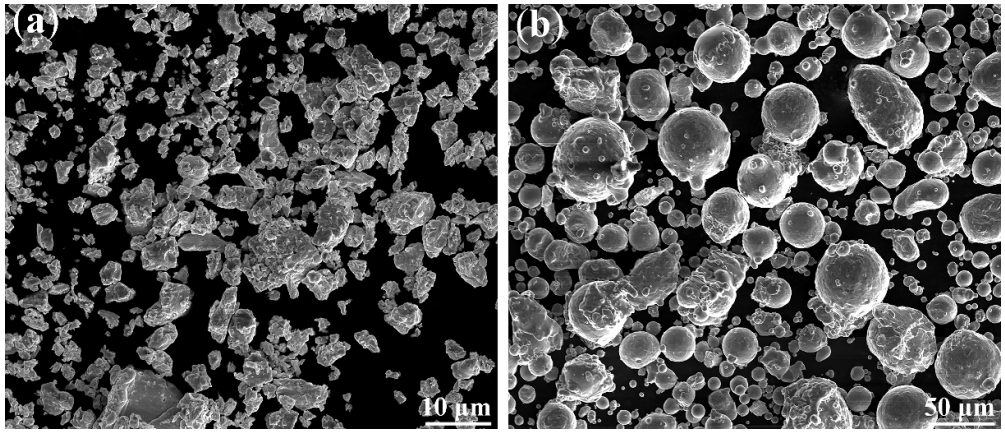

Fig. 1. Morphology of pure Zr powders (a) and Al-Cu-Mg powders with 2 wt.% Zr addition (b).

SLM processing

The SLM experiments were conducted on a self-developed machine (LSNF-I) whose details have been given elsewhere[15, 16]. All samples were deposited on the commercially AA 2024 substrate in an argon environment with the concentrations of H2O and O2 controlled well below 20 ppm. The SLM processing parameters of cubic samples were given in Table 1.

Table 1 SLM processing parameters used in the experiments.

Experiment	Parameters	Value
Cubic samples	Laser power (*P*, W)	200
	Dimensions (mm^3)	5*5*5
	Scanning speed (*V*, m/min)	5, 10, 15, 20, 25 and 30
	Hatching space (*HP*, μm)	60, 70, 80 and 90
	Layer thickness (*D*, μm)	40
	Scanning strategy (θ, °)	90

Characterization

The particle size was measured using the Malvern UK Mastersizer 3000. The relative density of the cubic specimens was evaluated by image processing of eight cross-section optical micrographs using ImagePro Plus 6.0 software. All samples were subjected to a standard metallographic procedure. For microstructure analysis, samples were etched by a solvent which consists of 2.5 mL HNO3, 1.5 mL HCl, 1 mL HF and 95 mL deionized water. The microstructure was characterized using an optical microscope (OM, EPIPHOT 300). The elements distribution of cubic samples was conducted by electron probe microanalyzer (EPMA). The surface roughness was obtained by using laser scanning confocal microscope (LSCM, KEYENCE VK-X200K).

Results and discussions

Formability

Fig. 2 shows the effect of scanning speed on the relative density of the selective laser melted (SLMed) samples (hatching space fixed at 90 μm). It is observed that the relative density decreases with the increase of scanning speed. Nearly fully dense samples were obtained when the scanning speed is low enough (5 m/min).

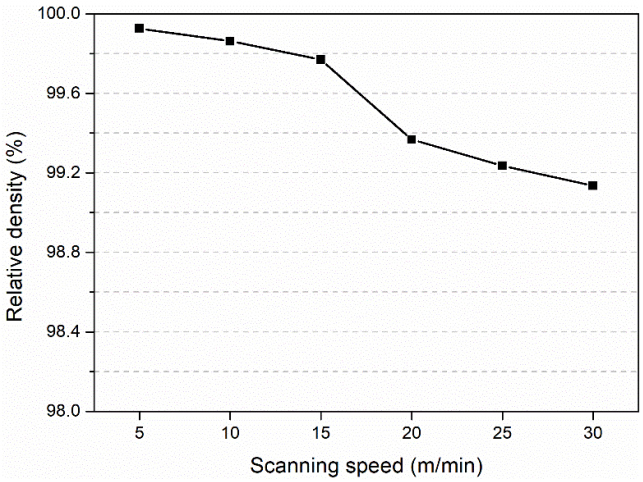

Fig. 2. Effect of scanning speed on the relative density.

Fig. 3 demonstrates the cross-sections of samples fabricated at different scanning speeds (hatching space fixed at 90 μm). The irregular pores occur when the scanning speed reaches to 20 m/min. The relative density significantly decreases when energy input is insufficient, that is, the scanning speed is too high to provide enough energy to melt adequate metal powders. Therefore, the irregular pores occur due to the weak connection between the layers and tracks.

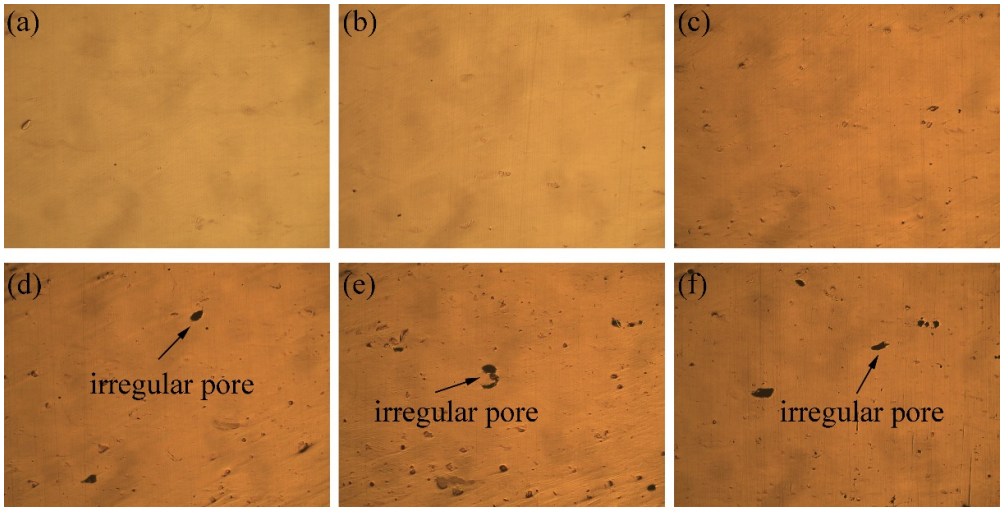

Fig. 3. Polished cross-sections of samples fabricated at different scanning speeds: (a) 5 m/min, (b) 10 m/min, (c) 15 m/min, (d) 20 m/min, (e) 25 m/min and (f) 30 m/min.

Fig. 4 shows the effect of hatching space on the relative density and surface roughness (scanning speed fixed at 10 m/min). From Fig. 4a-d, as the hatching space increases, the samples still fully dense. It clearly shows that the percentage of overlapping is adequate to guarantee the connection between the tracks. As far as surface roughness concerned, small hatching space (less than 70 μm) leads to high energy input and coarse surface with many metal balls, as shown in Fig. 4e and f. It is suggested that small hatching space enables the track fabricated previously to receive more energy and has preheating function to the following tracks, which generates the excessive size of the melt pool, therefore, balling phenomenon occurs. The surface roughness of samples fabricated at 60, 70, 80 and 90 μm are 10.47, 8.44, 6.97 and 6.46 μm, respectively. Taking into consideration the relative density, processing efficiency and surface roughness, the optimal processing parameters are laser power of 200 W, hatching space of 90 μm, layer thickness of 40 μm, and scanning speed of 10 m/min.

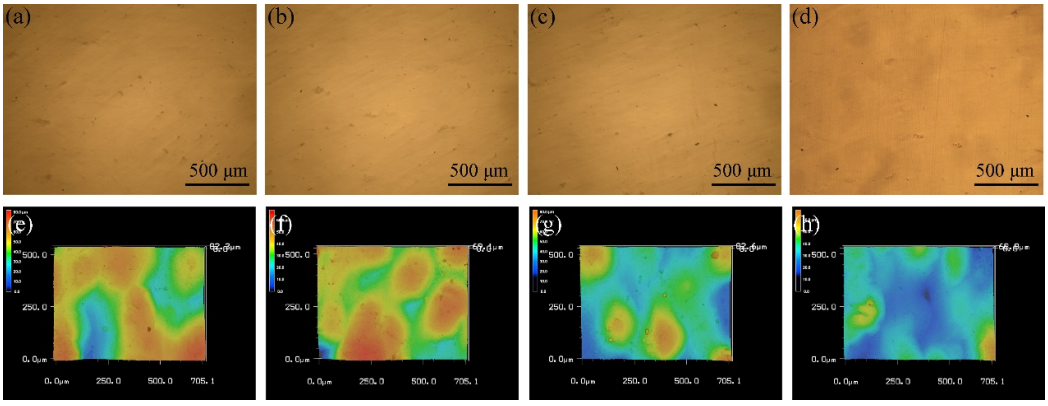

Fig. 4. Polished cross-sections and 3D images of samples fabricated at different hatching spaces (scanning speed fixed at 10 m/min): (a, e) 60 μm, (b, f) 70 μm, (c, g) 80 μm and (d, h) 90 μm.

Microstructure

Fig. 5 shows the microstructure of samples fabricated with different scanning speeds. The distribution of equiaxed grains is homogenous when the scanning speed is 5 m/min, as presented in Fig. 5a. Fig. 5b-c shows the typical bi-modal microstructure, that is, the fine equiaxed grains intersperse with coarse grains. However, the flow of molten metal is much more unstable when the scanning speed is above 15 m/min, as shown in Fig.5 d-f. More details can be found in the work of H. Zhang [14]. The boundary of melt pool becomes blurry due to the unstable flow. What's more, the grain size slightly decreases with the increase of scanning speed. High scanning speed leads to the high cooling rate, which contributes to the refinement of grains.

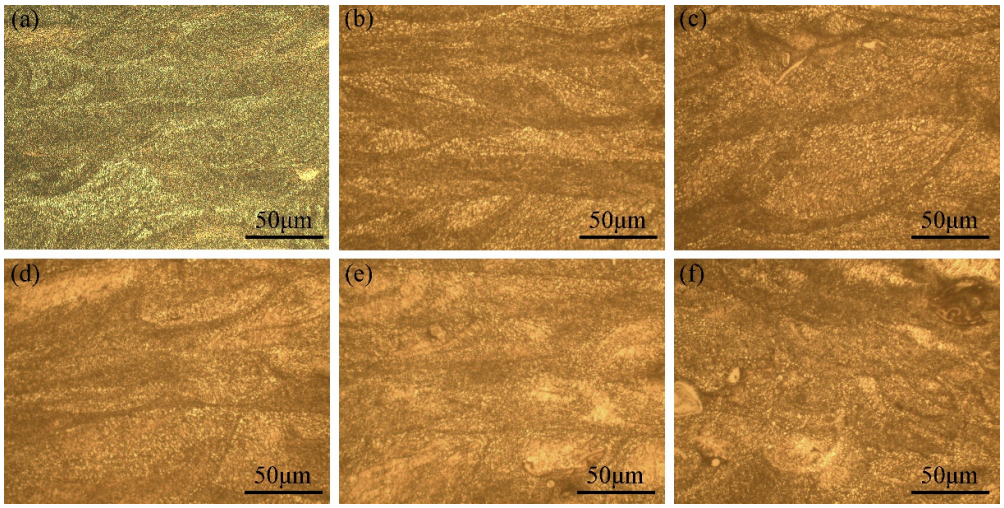

Fig. 5. Microstructure of SLMed samples fabricated with different scanning speeds: (a) 5 m/min, (b) 10 m/min, (c) 15 m/min, (d) 20 m/min, (e) 25 m/min and (f) 30 m/min.

Element distribution

Fig. 6 illustrate the distribution of elements in the SLMed samples fabricated at 10 m/min. It is clearly demonstrated that Cu and O elements are mainly enriched in the grain boundaries (Fig. 6b and e). In addition, Zr element is enriched in the junction of larger equiaxed grains and fine equiaxed grains, as illustrated in Fig. 6d. It is worth noting that little zirconium oxides can be observed in the grains.

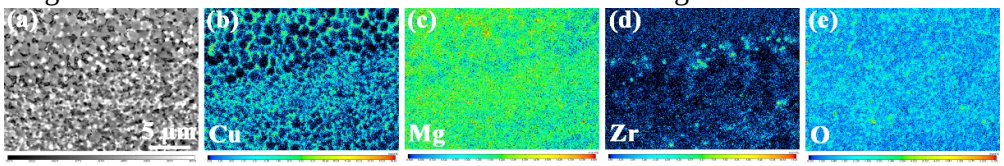

Fig. 6. Quantitative chemical maps obtained using EPMA in the cross-section of samples fabricated at 10 m/min.

Conclusions

Effect of scanning speed and hatching space on the relative density and surface roughness of SLMed 2 wt.% modified Al-Cu-Mg alloy was investigated. With the increase of the scanning speed, the relative density decreases. The hatching space influences the surface roughness of samples. The smaller hatching space, the coarser

the surface roughness. The microstructure is affected by the scanning speed. The distribution of fine equiaxed grains transforms from homogenous to bi-modal due to the increase of the scanning speed. Al_3Zr and ZrO particles serve as the nucleate during the solidification.

Future works

As that the suitable heat treatment is necessary for the SLMed samples is proposed. The future works may concentrate on the influence of the heat treatment on the SLMed Zr modified Al-Cu-Mg alloy.

Acknowledgements

This research is supported by the National Natural Science Foundation of China (61475056) and the National Program on Key Basic Research Project of China (613281). The authors would like to thank the Analytical and Testing Center of HUST.

References

[1] A.B. Spierings, K. Dawson, P.J. Uggowitzer, K. Wegener, Influence of SLM scan-speed on microstructure, precipitation of Al 3 Sc particles and mechanical properties in Sc- and Zr-modified Al-Mg alloys, Materials & Design, 140 (2018) 134-143.

[2] N. Kang, P. Coddet, Q. Liu, H. Liao, C. Coddet, In-situ TiB/near α Ti matrix composites manufactured by selective laser melting, Additive Manufacturing, 11 (2016) 1-6.

[3] B. Vrancken, L. Thijs, J.P. Kruth, J. Van Humbeeck, Microstructure and mechanical properties of a novel β titanium metallic composite by selective laser melting, Acta Materialia, 68 (2014) 150-158.

[4] R. Pérez-Bustamante, M.J. González-Ibarra, J. González-Cantú, I. Estrada-Guel, J.M. Herrera-Ramírez, M. Miki-Yoshida, R. Martínez-Sánchez, AA2024–CNTs composites by milling process after T6-temper condition, Journal of Alloys and Compounds, 536 (2012) S17-S20.

[5] C. Carreño-Gallardo, I. Estrada-Guel, M. Romero-Romo, R. Cruz-García, C. López-Meléndez, R. Martínez-Sánchez, Characterization of Al2O3NP–Al2024 and AgCNP–Al2024 composites prepared by mechanical processing in a high energy ball mill, Journal of Alloys and Compounds, 536 (2012) S26-S30.

[6] M.L. Montero Sistiaga, R. Mertens, B. Vrancken, X. Wang, B. Van Hooreweder, J.-P. Kruth, J. Van Humbeeck, Changing the alloy composition of Al7075 for better processability by selective laser melting, Journal of Materials Processing Technology, 238 (2016) 437-445.

[7] J. Liu, P. Yao, N. Zhao, C. Shi, H. Li, X. Li, D. Xi, S. Yang, Effect of minor Sc and Zr on recrystallization behavior and mechanical properties of novel Al–Zn–Mg–Cu alloys, Journal of Alloys and Compounds, 657 (2016) 717-725.

[8] V.V. Zakharov, EFFECT OF SCANDIUM ON THE STRUCTURE AND PROPERTIES OF ALUMINUM ALLOYS.pdf, Metal Science and Heat Treatment, (2003).

[9] S. Dev, A.A. Stuart, R.C.R.D. Kumaar, B.S. Murty, K.P. Rao, Effect of scandium

additions on microstructure and mechanical properties of Al–Zn–Mg alloy welds, Materials Science and Engineering: A, 467 (2007) 132-138.
[10] Y. Shi, P. Rometsch, K. Yang, F. Palm, X. Wu, Characterisation of a novel Sc and Zr modified Al–Mg alloy fabricated by selective laser melting, Materials Letters, (2017).
[11] S. Griffiths, M.D. Rossell, J. Croteau, N.Q. Vo, D.C. Dunand, C. Leinenbach, Effect of laser rescanning on the grain microstructure of a selective laser melted Al-Mg-Zr alloy, Materials Characterization, (2018).
[12] A.B. Spierings, K. Dawson, K. Kern, F. Palm, K. Wegener, SLM-processed Sc- and Zr- modified Al-Mg alloy: Mechanical properties and microstructural effects of heat treatment, Materials Science and Engineering: A, 701 (2017) 264-273.
[13] A.B. Spierings, K. Dawson, P. Dumitraschkewitz, S. Pogatscher, K. Wegener, Microstructure characterization of SLM-processed Al-Mg-Sc-Zr alloy in the heat treated and HIPed condition, Additive Manufacturing, 20 (2018) 173-181.
[14] H. Zhang, H. Zhu, X. Nie, J. Yin, Z. Hu, X. Zeng, Effect of Zirconium addition on crack, microstructure and mechanical behavior of selective laser melted Al-Cu-Mg alloy, Scripta Materialia, 134 (2017) 6-10.
[15] X. Nie, H. Zhang, H. Zhu, Z. Hu, L. Ke, X. Zeng, Analysis of processing parameters and characteristics of selective laser melted high strength Al-Cu-Mg alloys: From single tracks to cubic samples, Journal of Materials Processing Technology, 256 (2018) 69-77.
[16] X. Han, H. Zhu, X. Nie, G. Wang, X. Zeng, Investigation on Selective Laser Melting AlSi10Mg Cellular Lattice Strut: Molten Pool Morphology, Surface Roughness and Dimensional Accuracy, Materials (Basel), 11 (2018).